



HAL
open science

Li 2.0 Ni 0.67 N: a promising negative electrode material for Li-ion batteries with a soft structural response

Thomas Cavoué, Nicolas Emery, Nurzhan Umirov, Stéphane Bach, Pascal Berger, Zhumabay Bakenov, Céline Cénac-Morthe, Jean Pierre Pereira-Ramos

► To cite this version:

Thomas Cavoué, Nicolas Emery, Nurzhan Umirov, Stéphane Bach, Pascal Berger, et al.. Li 2.0 Ni 0.67 N: a promising negative electrode material for Li-ion batteries with a soft structural response. Inorganic Chemistry, 2017, 56, pp.13815-13821. 10.1021/acs.inorgchem.7b01903 . cea-01626781

HAL Id: cea-01626781

<https://cea.hal.science/cea-01626781>

Submitted on 31 Oct 2017

HAL is a multi-disciplinary open access archive for the deposit and dissemination of scientific research documents, whether they are published or not. The documents may come from teaching and research institutions in France or abroad, or from public or private research centers.

L'archive ouverte pluridisciplinaire **HAL**, est destinée au dépôt et à la diffusion de documents scientifiques de niveau recherche, publiés ou non, émanant des établissements d'enseignement et de recherche français ou étrangers, des laboratoires publics ou privés.

Li_{2.0}Ni_{0.67}N: a promising negative electrode material for Li-ion batteries with a soft structural response

Thomas Cavoué[†], Nicolas Emery^{*,†}, Nurzhan Umirov[‡], Stéphane Bach^{†,§}, Pascal Berger[‡], Zhumabay Bakenov[‡], Céline Cénac-Morthe[‡] and Jean-Pierre Pereira-Ramos[†]

[†]Institut de Chimie et Matériaux Paris-Est, UMR 7182 CNRS-UPEC, 2 rue Henri Dunant, 94320 Thiais, France

[‡]Institute of Batteries LLC, Nazarbayev University, 53 Kabanbay Batyr Avenue, Astana 010000, Kazakhstan

[§] Univ. d'Evry Val d'Essonne, Bd F. Mitterrand, Département Chimie, 91025 Evry Cedex, France

[‡]NIMBE, CEA, CNRS, Université Paris-Saclay, CEA Saclay, 91191 Gif sur Yvette Cedex, France

[‡]CNES, 118 Avenue Edouard Belin, 31401 Toulouse Cedex 9, France

ABSTRACT: The layered lithium nitridonickelate Li_{2.0(i)}Ni_{0.67(2)}N have been investigated as negative electrode in the 0.02-1.25 V vs. Li⁺/Li potential window. Its structural and electrochemical properties are reported. *Operando* XRD experiments upon three successive cycles clearly demonstrate a single phase behavior in line with the discharge-charge profiles. The reversible breathing of the hexagonal structure, implying a supercell, is fully explained. The Ni²⁺/Ni⁺ redox couple is involved and the electron transfer is combined with the reversible accommodation of Li⁺ ions in the cationic vacancies. The structural response is fully reversible and minimal, with a maximal volume variation of 2%. As a consequence, a high capacity of 200 mAh g⁻¹ at C/10 is obtained with an excellent capacity retention, close to 100% even after 100 cycles, which makes Li_{2.0(i)}Ni_{0.67(2)}N a promising negative electrode material for Li-ion batteries.

Introduction

Lithium transition metal nitrides attract tremendous attention for energy storage application as Li-ion negative electrode materials^{1,2} due to their low operating voltage.³ Among the lamellar phases, lithium cobalt nitrides with general chemical formula Li_{3-x-y}Co_xN (y is the vacancy amount in the cationic network) was the subject of lot of efforts.⁴⁻⁹ From the first works of Shodai et al⁵ and Nishijima et al⁶ the ternary compound Li_{2.6}Co_{0.4}N was proved to be the most promising material with a large capacity in the range 480-860 mAh g⁻¹ in the potential window 0.02-1.4 V vs. Li⁺/Li. However, such great capacities are due to conversion reaction with a poor capacity retention. More recently, Ducros et al⁷⁻⁹ focused their investigation in a narrower potential window (0.02-0.85 V vs. Li⁺/Li) and demonstrated that these lithium cobalt nitrides Li_{3-x-y}Co_xN can operate as genuine Li intercalation compounds. As a result, specific capacities up to 180 mAh g⁻¹ were attained with excellent cycling life.^{7,8}

The group of lithium nitridonickelate Li_{3-x-y}Ni_xN (0 < x < 0.6) has been prepared and investigated.^{8,10} In particular, their structural and electrochemical behavior have been studied as a function of the nickel content. In the potential range 0.02-1 V vs. Li⁺/Li, the best stable specific capacity reaches 160 mAh g⁻¹ for Li_{1.86}Ni_{0.57}N, assuming a +2 valence of nickel ions.^{8,10} To still increase the available capacity, Cabana et al¹¹ evaluated the peculiar ternary LiNiN, which potentially encloses more active redox center due to a higher nickel content. However, in the 0.02-1 V potential range, the delivered specific capacity only reached 160 mAh g⁻¹. In

spite of attractive characteristics like a single redox step around 0.5 V, a high rechargeability upon cycling and a low hysteresis between discharge and charge (< 100 mV)^{8,10}, no attention has been paid to the improvement of lamellar lithium nitridonickelates electrochemical properties. In addition, the structural understanding of this anode material upon successive reduction and oxidation cycles has never been undertaken.

The aim of the present work is to provide more information about the electrochemical lithium insertion into the nitride Li_{2.0(i)}Ni_{0.67(2)}N in the 0.02-1.25 V potential range and the related structural mechanism. We will examine the structure evolution induced by lithium insertion-extraction in this ternary nitride using in *Operando* XRD. The cycling properties of the material will be analyzed and discussed on the basis of these new data.

Experimental

Due to the moisture sensitive character of lithium nitride derivatives, all the manipulations were performed under controlled atmosphere. During our synthesis procedure, starting materials and reaction products are not exposed to ambient atmosphere. Li_{2.0(i)}Ni_{0.67(2)}N has been prepared through solid state reaction in nitrogen (N₂). Around 2 g of a mixture of Li₃N (alfa aesar, 99.4% metal basis) and nickel powders (molar ratio Ni/Li₃N = 1) was thoroughly ground in an agate mortar then die-pressed into pellet. Once arranged in an alumina crucible, the sample was transferred into a specially designed stainless steel reactor, which allowed to perform thermal treatment at 720°C under continuous N₂ flux for 12 h. To trap any possible oxygen

traces present in nitrogen gas, the sample was surrounded by crucibles filled with titanium sponge.

Quantitative analysis of nickel in the as prepared sample was performed by complexometric titration with EDTA in basic media. Powder was first mineralized in nitric acid solution and then pH was adjusted up to 9 by addition of NH_4OH (30%) solution. Murexide indicator used for titration is highly colored and complexes with nickel ions give yellow species. During the titration, EDTA forms a more stable complex than the murexide. As a consequence, the indicator is released in the solution and displays its original blue color in basic media. The appearance of the free indicator means that all metal ions have been complexed by EDTA and signals the end point of the titration.

Further, the complete chemical composition was determined through ion beam analysis (IBA), including Rutherford Back Scattering (RBS) and Nuclear Reaction Analysis (NRA). IBA experiment was performed with a 3.03 MeV H^+ beam produced by the Van de Graaf accelerator of the IRAMIS/LEEL at CEA-Saclay and the spectrum was collected using an annular detector, which covers back scattering angles centered around 170° .

Electrochemical tests were performed in two electrodes configuration using CR2032 coin cells on a Biologic VMP3 potentiostat. The working electrode was composed of a mixture of active material (80 wt%), Carbon Super P (10 wt%, conductive agent) and PTFE (10 wt%, binder) pressed on a copper grid. A metallic lithium disk was used as counter electrode and the separator was silica glass fibers paper (Whatmann) soaked with LP71 electrolyte (EC:DEC:DMC, LiPF_6 1 mol L^{-1} , BASF).

All the X-ray diffraction patterns in the present work were collected using a Panalytical X'Pert Pro diffractometer using a cobalt radiation and equipped with an X'celerator rapid detector. The as-prepared powder was studied using an air-tight polymer sample holder while the *operando* XRD acquisitions were performed using a homemade two-electrode electrochemical cell described elsewhere.¹² All the diffraction patterns were analyzed using GSAS+EXPGui package^{13,14} with the Rietveld method. In the case of the *operando* pattern, environment contributions like Be window or the copper grid were fitted with the Le Bail method.

The structural response of $\text{Li}_{2.0(i)}\text{Ni}_{0.67(2)}\text{N}$ has been studied by *operando* X-ray diffraction using the same composition of working electrode as for electrochemical tests. In this experiment, the supporting copper grid was directly arranged on the beryllium window which acted as both current collector and X-ray transparent window. Full reduction/oxidation cycles were performed at C/20 rate (i.e. 1 Li^+ exchanged in 20h) using a Biologic VSP150 apparatus.

Results and Discussion

Synthesis product and its composition

The XRD pattern of the pristine powder is displayed in Figure 1. All peaks are easily indexed as Li_3N -type hexagonal structure ($P6/mmm$ space group)^{15,16} with the unit cell parameters $a = 3.760(1)$ Å and $c = 3.538(1)$ Å. In such a structure (inset of Figure 1), nitrogen ions are in **1a** site (blue spheres), while nickel ions (red spheres) and lithium ions (green spheres) fill the **1b** site. The **2c** site is partially occupied by lithium ions. The amount of vacancies in **2c** is directly related to the valence and the amount of nickel ions incorporated in the **1b** site. For a Ni^{2+} valence, which is usually the maximum valence for the transition metal in these lithium nitridometallates,¹⁵⁻¹⁸ the maximum amount of vacancies in the **2c** site is achieved and reaches the amount of nickel ions. As a result, the $(\text{Li}_{1-x}\text{Ni}_x)\text{N}$ chains formed by the **1a** and **1b** sites are always fully occupied and the chemical formula can be written $\text{Li}_{2-2x}\square_x[(\text{Li}_{1-x}\text{Ni}_x)\text{N}]$.

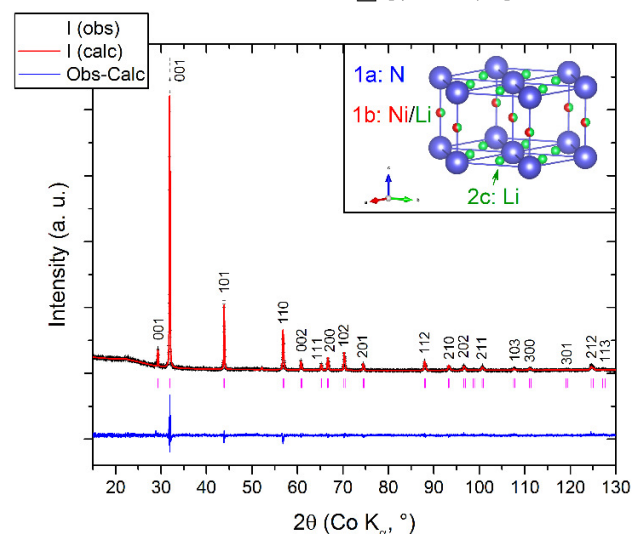


Figure 1. XRD pattern and Rietveld refinement of the $\text{Li}_2\text{Ni}_{0.67}\text{N}$ pristine powder ($\chi^2=1.15$, $\text{Rp}=8.9\%$, $\text{Rwp}=11.7\%$). Inset, representation of the Li_3N -type structure.

The complexometric titration of the mineralized sample by EDTA leads to a nickel weight percentage of 58.5. According to the literature¹⁵⁻¹⁸, nickel ions adopt mean valences between +1 and +2. It leads to a wide range of chemical composition, between $\text{Li}_{2.28}\text{Ni}_{0.72}\text{N}^{3-}$ (or $\text{Li}_2^+[(\text{Li}_{0.28}^+\text{Ni}_{0.72}^+)\text{N}^{3-}]$ to figure the $(\text{Li}_{1-x}\text{Ni}_x)\text{N}$ solid chains), and $\text{Li}_{1.74}\square_{0.63}\text{Ni}_{0.63}^{2+}\text{N}^{3-}$ (or with only vacancies in **2c** $\text{Li}_{1.37}\square_{0.63}[(\text{Li}_{0.37}^+\text{Ni}_{0.63}^{2+})\text{N}^{3-}]$), for the same weight percentage of nickel. To solve this issue, a piece of as-sintered pellet has been analysed by Ion Beam Analysis (see **Supplementary Materials SM 1**). The resulting composition was $\text{Li}_{2.0(i)}\text{Ni}_{0.67(2)}\square_{0.33}\text{N}$ ($\text{Li}_{1.67}\square_{0.33}[(\text{Li}_{0.33}\text{Ni}_{0.67})\text{N}]$), which corresponds to an intermediate valence for nickel ions close to +1.5(1) with 0.33 lithium vacancy in the $\text{Li}_{2-y}\text{N}^{(1-y)-}$ plane.

Electrochemical properties

Typical galvanostatic cycles of $\text{Li}_{2.0(i)}\text{Ni}_{0.67(2)}\text{N}$ at various cycling rates in the potential window 0.02-1.25V vs Li/Li^+ are displayed in Figure 2a. In good accordance with Ducros et al,¹⁰ sloping curves are evidenced with a single reduction

or oxidation step around 0.5 V of at any rate. When applying a low current density such as C/20 rate, a very small hysteresis was observed, lower than 100 mV. A specific capacity up to 210 mAh g⁻¹, corresponding to a faradaic yield of 0.53 F mol⁻¹, is achieved at C/20 rate. At a higher current density of C/2, around 55% of the specific capacity (~115 mAh g⁻¹) are still available (Figure 2a). Furthermore, an excellent cycling life was observed, with a specific capacity of 200 mAh g⁻¹ after more than 100 cycles at C/10 (Figure 2b). An outstanding coulombic efficiency of 100 % explained the high capacity retention upon extended cycling experiments, even after applying higher C rate over several cycles. The high and stable capacity of 200 mAh g⁻¹ is the highest value recorded for lithium nitridonickelates with an insertion mechanism.

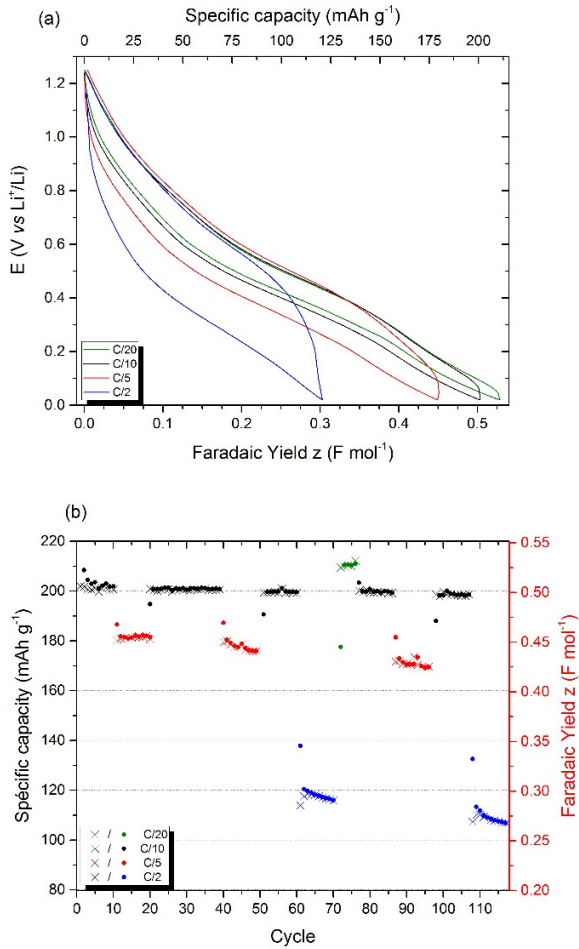


Figure 2. (a) typical galvanostatic cycles at various rates (C/2, C/5, C/10 and C/20) and (b) evolution of the specific capacity (reduction x; oxidation •) versus number of cycles at various rates.

Structural response upon cycling

The structural response upon discharge-charge cycling of Li_{2.0(1)}Ni_{0.67(2)}N has been studied using *operando* XRD experiments. The full data set, collected during the first 3 cycles, are available in **Supplementary Materials SM 2**. The first XRD pattern of Li_{2.0}Ni_{0.67}N electrode before cycling is

displayed in Figure 3 and experimental setup peaks are indexed in blue (copper grid and beryllium window). Most of the remaining peaks are indexed as the Li₃N-type hexagonal structure (space group *P6/mmm*, indexation in *hkl*^{*}) with the following cell parameters: *a* = 3.729 (1) Å and *c* = 3.556 (1) Å. These values are slightly different from the pristine powder (*a* = 3.760 (1) Å and *c* = 3.538 (1) Å) and suggest that a chemical oxidation took place during the electrode preparation. Indeed, even with drastic precautions used during handling and manipulations (acetylene black dried under argon atmosphere at 800°C, PTFE dried overnight at 200°C under primary vacuum, all manipulations performed under high purity argon atmosphere), such a reaction cannot be avoided. This kind of oxidation has already been evidenced in similar lamellar phases Li_{3-γ}Fe_γN through Mössbauer measurements¹⁹ and was attributed to the reactivity of the PTFE binder.^{20,21}

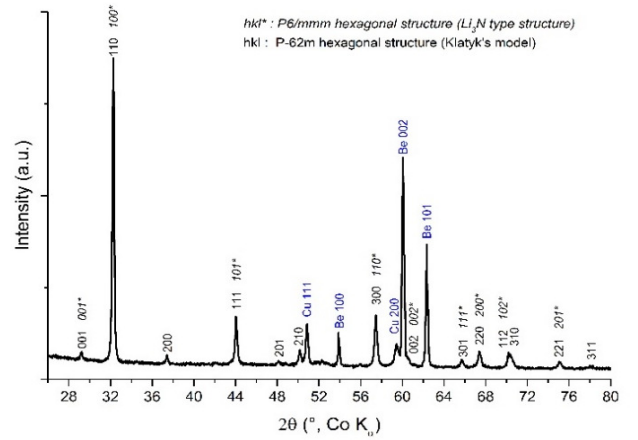


Figure 3. XRD pattern of Li₂Ni_{0.67}N electrode before cycling. Indexations *hkl*^{*} are related to the Li₃N-type structure while *hkl* indexations belonging to the *P6̄2m* supercell. Peaks ascribed to the experimental setup (Be window and copper grid) are indexed in blue.

Table 1. Description of the Li₃N-type structure adopted by Li₂Ni_{0.67}N within the *P6/mmm* and the *P6̄2m* space groups. The appropriate splitting of the Wyckoff position is evidenced.

Atom	Li ₃ N-type structure (<i>a</i> and <i>c</i> , <i>P6/mmm</i>)			Li ₅ [(Li _{0.23} Ni _{0.77})N] ₃ -type structure (<i>a</i> ' = <i>a</i> ·3 ^{1/2} and <i>c</i> , <i>P6̄2m</i>)				
	Site	x	y	Z	Site	x	y	z
Ni/Li	1b	0	0	1/2	3g	(^{X_w} =2/3)	0	0
N	1a	0	0	0	3f	(^{X_w} =2/3)	0	1/2
					3f	(^{X_w} =1/3)	0	0
Li	2c	1/3	2/3	0	2c	1/3	2/3	0
					1a	0	0	0

Compared to the pristine powder (Figure 1), a careful examination of this XRD electrode pattern (Figure 3) shows small additional peaks at 37.4, 48.1 and 50.1°. All of them can be indexed using a three time larger hexagonal unit cell, with $a' = 3^{1/2} \cdot a = 6.459 \text{ \AA}$. According to Klatyk et al.,²² the parent compound $\text{Li}_5[(\text{Li}_{1-y}\text{Ni}_y)\text{N}]_3$ (with $y = 0.77$, i.e. $\text{Li}_{1.90}\text{Ni}_{0.77}\text{N}$) adopted a similar unit cell, with a structure belonging to the space group $P\bar{6}2m$. The corresponding indexation is labelled hkl on Figure 3. $\text{Li}_5[(\text{Li}_{0.23}\text{Ni}_{0.77})\text{N}]_3$ structure is closely related to the Li_3N one since it can be seen as an ordered vacancies model of the basic Li_3N $P6/mmm$ structure. As for the Li_3N structure, the $(\text{Li}_{1-x}\text{Ni}_x)\text{N}$ chains are present and do not accommodate vacancies. All the voids are located in the Li_2N^- planes, inducing small displacement in the ab plane of the $(\text{Li}_{0.23}\text{Ni}_{0.77})\text{N}$ chains. It is clearly evidenced in Figure 4 where the ab plane representations of both $P6/mmm$ and $P\bar{6}2m$ structures are plotted. This allows to describe the Li_3N -type structure using the three-time larger hexagonal $P\bar{6}2m$ unit cell adopted by $\text{Li}_5[(\text{Li}_{0.23}\text{Ni}_{0.77})\text{N}]_3$ with the appropriate atomic position splitting displayed in Table 1. A similar structure relation between the $P6/mmm$ structure and the $P\bar{6}2m$ one has been described in the Li-Mn-N ternary system.²³

Therefore the $1b$ and $1a$ sites of $P6/mmm$ structure are replaced by $3g$ and $3f$ sites in $P\bar{6}2m$ structure, respectively. The difference of site multiplicities between these two models is simply due to their different unit cell volume. The case of the $2c$ site of $P6/mmm$ structure is slightly different. In the Klatyk model,²² three different positions are needed in the lower symmetry structure to describe the lithium network since the $2c$ site is split into $3f$, $2c$ and $1a$. In the original description of $\text{Li}_5[(\text{Li}_{0.23}\text{Ni}_{0.77})\text{N}]_3$, $1a$ site remains vacant since in nickel-substituted Li_3N some lithium vacancies are induced in the Li_2N^- plane to compensate the higher oxidation state of Ni ion regards to Li^+ ion. These vacancies are labelled V in Figure 4. Also, regards to the $P6/mmm$ structure, the $P\bar{6}2m$ one presents additional degrees of freedom for the $3g$ and $3f$ Wyckoff positions. Indeed, to accommodate the distortion of the Li_2N^- and Ni/Li planes induced by the vacancies, ions in these sites must slightly displaced in the ab plane regards to the highly symmetric structure $P6/mmm$ along the small vectors plotted in Figure 4b. According to the original model of Klatyk,²² x_w values of $3g$ and $3f$ of Ni/Li and N^{3-} ions were constrained to the same value in the Rietveld refinement procedure. Attempt to remove such a constraint has not led to drastically different values nor significant improvements of the fit. The Rietveld refinement of the electrode pattern before cycling, presented in **Supplementary Materials SM 3**, leads to an x_w value of 0.638(1). These small displacements from the peculiar $2/3$ position, limited to $\sim 0.2 \text{ \AA}$, lead to the reduction of the structure symmetry and induce the above mentioned additional diffraction peaks observed at 37.4, 48.1 and 50.1° (Figure 3). Although the vacancy model allows explaining the displacement of nickel and nitrogen ions, the X-ray diffraction data cannot let us to fully ascribe

lithium site occupancies or positions due to its low scattering factor. Indeed, we cannot ruled out the presence of vacancies in the other lithium sites.

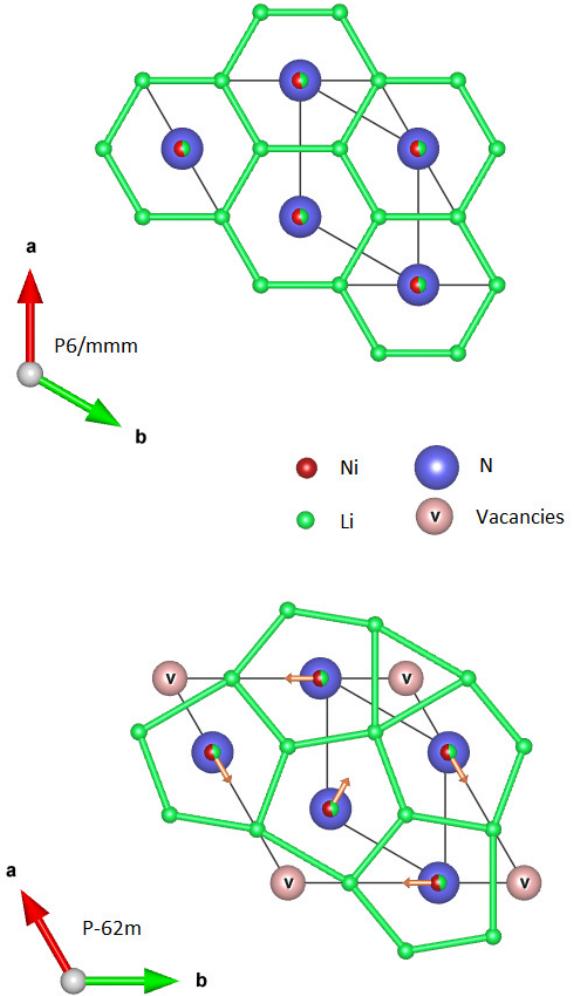


Figure 4. In-plane representation of the Li_3N -type and $\text{Li}_5[(\text{Li}_{1-x}\text{Ni}_x)\text{N}]_3$ -type structures. $\text{Li}_5[(\text{Li}_{1-x}\text{Ni}_x)\text{N}]_3$ -type is a superstructure of the Li_3N -type and the introduction of 1 vacancy in the Li_2N^- plane induces the rearrangement of lithium ions and a displacement of nickel and nitrogen ions along the small vectors regards to the original Li_3N -type structure.

Three full reduction oxidation cycles were accompanied with *Operando* XRD and the full data set is presented in **Supplementary Materials SM 2**. As it is commonly observed in this potential range, it can be confirmed that the first reduction process exhibited an extra capacity due to the SEI (Solid Electrolyte Interface) formation with the carbon black conducting agent. Therefore, the discussion on structural response is focused on the second full cycle, which is free of such irreversible redox phenomenon (Figure 5). Also, in order to simplify the discussion, all the following indexations belonging to the $\text{Li}_5[(\text{Li}_{0.23}\text{Ni}_{0.77})\text{N}]_3$ -type supercell ($P\bar{6}2m$ space group) are given as “hkl” while those related to the $P6/mmm$ structure are reported as “hkl*”.

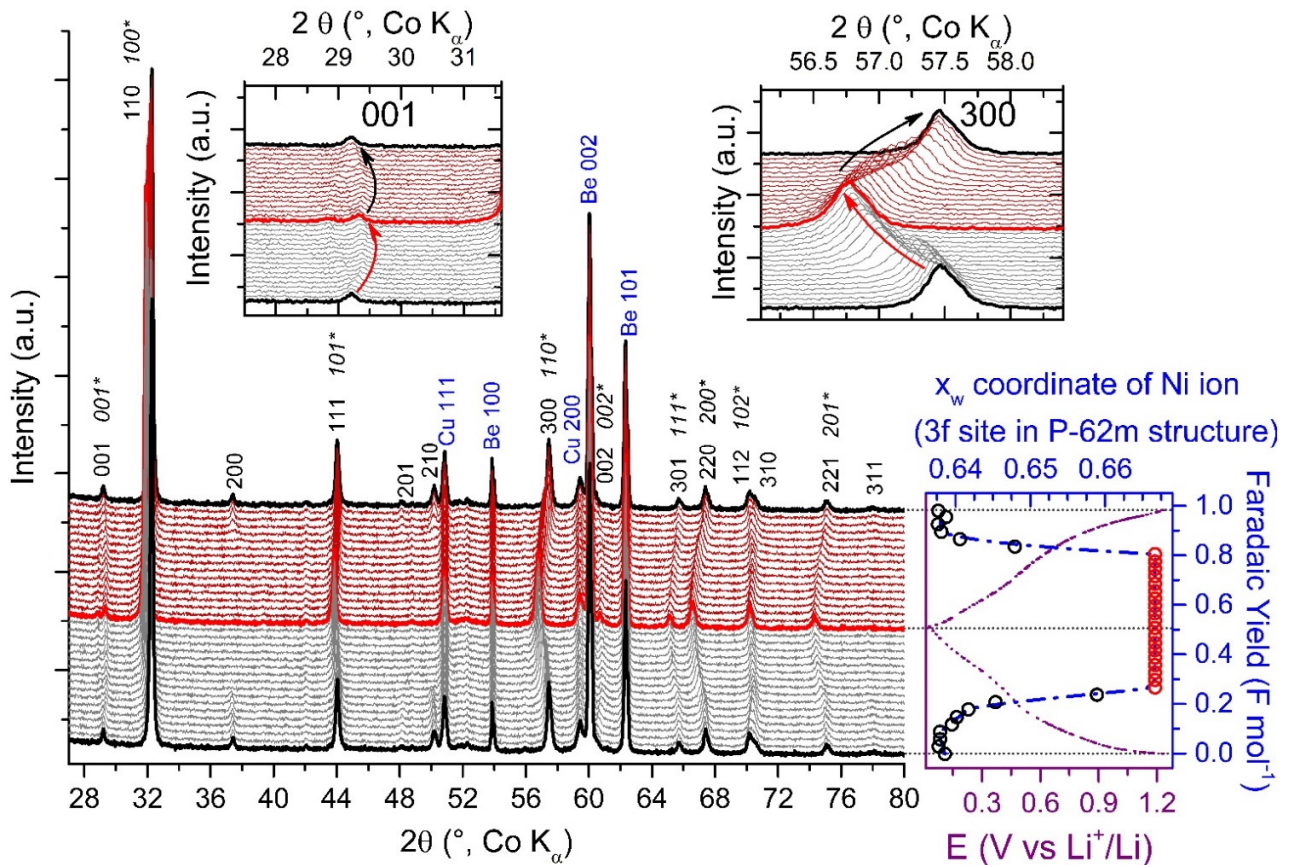


Figure 5. Left panel represents the second full reduction/oxidation cycle. hkl^* Indexations are related to the Li_3N -type structure while hkl indexations belonging to the $P\bar{6}2m$ supercell. Peaks ascribed to the experimental setup (Be window and copper grid) are indexed in blue. Insets, displacement of the 001 and 300 diffraction peaks ($P\bar{6}2m$ indexation). Right panel displays the associate electrochemical curve and x_w Wyckoff position evolution in the $P\bar{6}2m$ supercell structure of nickel ion.

Two main features are observed upon electrochemical reduction (Figure 5):

- i) Supercell peaks 200, 201 and 210 gradually vanish and completely disappear for a faradaic yield z of ~ 0.26 . As a consequence, for z between 0 and 0.26, XRD data are described using the supercell structure ($P\bar{6}2m$) while for higher Li uptake ($0.26 < z < 0.53$), the simple Li_3N -type structure ($P6/mmm$) fully indexes the XRD patterns.
- ii) Simultaneously, in-plane and out-of-plane cell parameters exhibit opposite gradual variations. Indeed, the hko related reflections gradually shift to lower angles, which indicates the dilation of the in-plane cell parameter a . It is particularly evident for the 110 (or 100^*), 300 (or 110^* , see inset of Figure 5) and 220 (or 200^*) reflections located at 32.3° , 57.4° and 67.4° , respectively. The evolution of the c parameter appears to be more complex and take place in two distinctive steps. Indeed, the inset focused on the 001 evolution shows first a gradual displacement to the higher angles with a maximum shift

for $z \sim 0.3$, indicating a contraction of the c parameter. Then, for $z > 0.3$, the 001 peak slightly shifts to the lower angles until the end of the reduction, sign of a small dilation in this second step.

The electrochemical oxidation demonstrates the full reversibility of these two main features (Figure 5). Indeed, the reverse shifts occur for all the diffraction lines previously mentioned. The supercell is restored with similar cell parameters at the end of the oxidation process (presence of the 200, 201 and 210 peaks). Rietveld refinements performed for each pattern allow us to provide a precise description of the above mentioned structural changes induced by these reduction/oxidation processes.

Firstly, the cell parameter variations have been determined and are plotted in Figure 6. Upon lithium insertion, a continuous dilation of the in-plane parameter a was evidenced from 3.728 \AA to 3.769 \AA , i.e. with an increase of 1.1%. In the same time, a contraction of the interlayer distance, i.e. the cell parameter c , is observed from 3.557 \AA down to 3.537 \AA between 0.2 and 0.35 F mol^{-1} . Then, a reverse trend is observed since it increases up to 3.545 \AA for a faradaic yield z included between 0.3 and 0.53 F mol^{-1} .

Therefore, the maximum amplitude of the c parameter was limited to only 0.6 %. Finally, the overall volume variation did not exceed 2 % after the reduction (Figure 6). Evolution of the cell parameters and cell volume determined from the XRD patterns registered upon the oxidation (Figure 5) fully confirmed the high reversibility of these structural variations since it is the symmetric of the reduction process (Figure 6). In addition, the third cycle (**Supplementary Materials SM 2**) could be considered as a replica of the second cycle, and the same structural evolution is demonstrated. This limited and highly reversible breathing of the structure must be correlated to the excellent cycling life illustrated in Figure 2b.

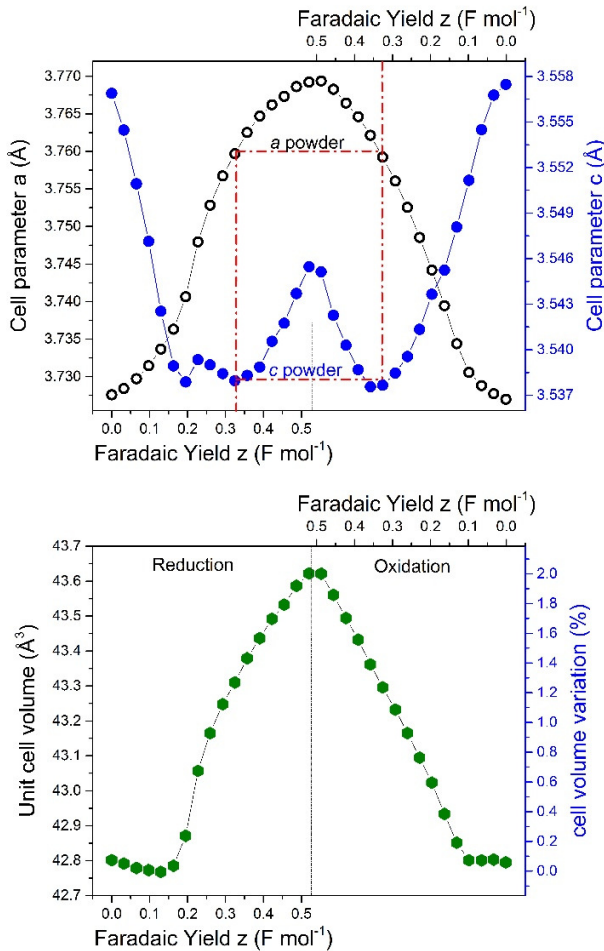


Figure 6. a and c cell parameter evolution during the full second cycle (in the $P6/mmm$ Li_3N -type structure) and evolution of the associate cell volume variation. To convert these values in the $P\bar{6}2m$ supercell structure, cell parameter a has to be multiply by $3^{1/2}$ and the volume by 3.

Secondly, the structural mechanism of lithium accommodation in $\text{Li}_{2.0(i)}\text{Ni}_{0.67(z)}\text{N}$ through electrochemical insertion / extraction has been precisely solved. During the reduction, the insertion of lithium in the cell leads to a rearrangement in the Li_2N^- plane, inducing the displacement of ions in **3f** and **3g**. Then, as shown in Figure 5, $(\text{Li}_{0.33}\text{Ni}_{0.67})\text{N}$ chains formed by nickel and nitrogen ions are moving from $x_w \approx 0.638$ to $x_w = 2/3$ during the reduction,

i.e. adopted again the Li_3N type structure. Therefore, Figure 5 evidences that the intensities of supercell peaks are directly related to the displacement of nickel and nitrogen ions. The oxidation process clearly demonstrates the reversibility of such a distortion, since the supercell reflections appear after extraction of $\sim 0.3 \text{ Li}^+$ per unit formula.

We have been able to build a relevant picture of the structural response of $\text{Li}_{2.0(i)}\text{Ni}_{0.67(z)}\text{N}$ upon electrochemical lithium insertion / extraction in the potential window 0.02-1.25 V vs Li^+/Li . However, variations of chemical composition have not yet been discussed. Due to the above mentioned reaction of PTFE binder by $\text{Li}_{2.0(i)}\text{Ni}_{0.67(z)}\text{N}$ and the formation of SEI during the first cycle, it was not possible to estimate the composition of $\text{Li}_x\text{Ni}_{0.67(z)}\text{N}$ only from coulometric titration in its most oxidized or reduced states. To fulfill this lack, the cell parameter evolution allows rescaling the faradaic yield variation. As it is indicated in Figure 6, upon reduction the unit cell parameters (a and c) of the pristine powder, for which the composition is clearly determined by IBA experiment, are recovered for a faradaic yield of 0.33 F mol^{-1} . This indicates that for this faradaic yield, the chemical composition is $\text{Li}_{2.0(i)}\square_{0.33}\text{Ni}_{0.67(z)}\text{N}$. Therefore, the composition of the most oxidized phase, for $z = 0$, should be close to $\text{Li}_{1.67}\square_{0.67}\text{Ni}_{0.67(z)}\text{N}$ (or $\text{Li}_4\square_2[(\text{Li}_{0.33}\text{Ni}_{0.67})\text{N}]_3$ according to Klatyck *et al* model). It is worth noticing that with a composition of $\sim \text{Li}_{1.67}\text{Ni}_{0.67(z)}\text{N}$, nickel ion adopts a +2 valence, with one lithium vacancy for each nickel ion. On the contrary, the reduction to a potential of 0.02 V vs. Li^+/Li does not allow to fully reduce nickel ions down to the +1 valence. Indeed, the corresponding chemical composition reaches $\sim \text{Li}_{2.20}\square_{0.15}\text{Ni}_{0.67(z)}\text{N}$ (or $\text{Li}_{1.87}\square_{0.15}[(\text{Li}_{0.33}\text{Ni}_{0.67})\text{N}]$), with ~ 0.15 remaining vacancies per unit formula in $2c$ site.

Conclusions

With a specific capacity of 200 mAh g⁻¹ at low potential (0.02 - 1.25 V vs. Li^+/Li) and an excellent capacity retention close to 100 % maintained over 100 cycles, $\text{Li}_{2.0(i)}\text{Ni}_{0.67(z)}\text{N}$ exhibits promising properties as negative electrode material for lithium-ion batteries. Such excellent cycling life is attributed to its structural response upon electrochemical lithiation. Indeed, based on in operando XRD, a complete picture of these mechanisms is provided. First, the structure breathing, implying limited and opposed a and c cell parameters variations, was reduced to less than 2%. Second, the creation of vacancies in the Li_2N^- plane by the electrochemical oxidation was accommodated by a smooth reorganization of lithium ions associated to a soft displacement in the ab plane of the $(\text{Li}_{0.33}\text{Ni}_{0.67})\text{N}$ solid chains. As a result, a hexagonal supercell with a three time larger volume was observed. In addition, the reduction process demonstrated the full reversibility of these deformations and, again, supported the excellent electrochemical properties of the system.

ASSOCIATED CONTENT

Supporting Information. IBA spectrum and his fit (SM 1), first Rietveld Refinement of the $\text{Li}_2\text{Ni}_{0.67}\text{N}$ electrode (SM 2) and the three first full electrochemical cycle (SM 3). These

materials are available free of charge via the Internet at
<http://pubs.acs.org>.

AUTHOR INFORMATION

Corresponding Author

* E-mail: emery@icmpe.cnrs.fr

REFERENCES

- (1) Cameron, J. M.; Hughes, R. W.; Zhao, Y.; Gregory, D. H. Ternary and higher pnictides; prospects for new materials and applications, *Chem. Soc. Rev.* **2011**, *40*, 4099-4118
- (2) Gregory, D. H. Lithium nitrides as sustainable energy materials, *Chem. Rec.* **2008**, *8*, 229-239
- (3) Suzuki, S.; Shodai, T. Electronic structure and electrochemical properties of electrode material $\text{Li}_{7-x}\text{MnN}_4$, *Solid State Ionics* **1999**, *116*, 1-9
- (4) Nishijima, M.; Kagohashi, T.; Imanashi, M.; Takeda, Y.; Yamamoto, O.; Kondo, S. Synthesis and electrochemical studies of a new anode material, $\text{Li}_{3-x}\text{Co}_x\text{N}$, *solid state ionics*, **1996**, *83*, 107-111
- (5) Shodai, T.; Okada, S.; Tobishima, S.I.; Yamanaki, J.I. Study of $\text{Li}_{3-x}\text{M}_x\text{N}$ (M: Co, Ni or Cu) system for use as anode material in lithium rechargeable cells, *Solid State Ionics* **1996**, *785-789*
- (6) Ducros, J.B.; Bach, S.; Pereira-Ramos, J.P.; Willmann, P. A novel lithium intercalation compound based on the layered structure of lithium nitridonickelates $\text{Li}_{3-2x}\text{Ni}_x\text{N}$, *Electrochim. Acta* **2007**, *52*, 7035-7041
- (7) Nishijima, M.; Kagohashi, T.; Takeda, Y.; Imanishi, M.; Yamamoto, O. Electrochemical studies of a new anode material $\text{Li}_{3-x}\text{M}_x\text{N}$ (M=Co, Ni, Cu), *J. Power Sources* **1997**, *68*, 510-514
- (8) Ducros, J.B.; Bach, S.; Pereira-Ramos, J.P.; Willmann, P. Layered lithium cobalt nitrides: a new class of lithium intercalation compounds, *J. Power Sources* **2008**, *175*, 517-525
- (9) Ducros, J.B.; Bach, S.; Pereira-Ramos, J.P.; Willmann, P. Optimization of cycling properties of the layered lithium cobalt nitride $\text{Li}_{2.20}\text{Co}_{0.40}\text{N}$ as negative electrode material for Li-ion batteries, *Electrochim. Acta* **2015**, *167*, 20-24
- (10) J.B. Ducros, S. Bach, J.P. Pereira-Ramos, P. Willmann, Comparison of the electrochemical properties of metallic layered nitrides containing cobalt, nickel and copper in the 1V – 0.02V potential range, *Electrochem. Com.* **9** (2009) 2496-2500
- (11) Cabana, J.; Stoeva, Z.; Titman, J. J.; Gregory, D. H.; Palacin, M. R. Toward new negative electrode materials for Li-ion batteries: Electrochemical properties of LiNiN , *Chem. Mater.* **2008**, *20*, 1676-1678
- (12) Panabière E., PhD Thesis, Université Paris-Est Créteil, 2013
- (13) Larson, A. C.; Von Dreele, R.B. General Structure Analysis System (GSAS), Los Alamos National Laboratory, Technical Report No. LAUR86-748, 2004
- (14) Toby, B. H. EXPGUI, a graphical user interface for GSAS, *J. Appl. Cryst.* **2001**, *34*, 210-221
- (15) Stoeva, Z.; Smith, R. I.; Gregory, D. H. Stoichiometry and defect structure control in the ternary lithium nitridometalates $\text{Li}_{3-x-y}\text{Ni}_x\text{N}$, *Chem. Mater.* **2006**, *18*, 313-320.
- (16) Niewa, R.; Huang, Z.-L.; Schnelle, W.; Hu, Z.; Knip, R. Preparation, Crystallographic, Spectroscopic and Magnetic Characterization of Low-Valency Nitridometalates $\text{Li}_2[(\text{Li}_{1-x}\text{M}_x)\text{N}]$ with M=Cu, Ni, *Z. Anorg. Allg. Chem.* **2003**, *629*, 1778-1786
- (17) Gregory, D.H.; O'Meara, P.M.; Gordon, A.G.; Hodges, J.P.; Short, S.; Jorgensen, J.D. Structure of lithium nitride and transition-metal-doped derivatives, $\text{Li}_{3-x-y}\text{M}_x\text{N}$ (M=Ni,Cu): a powder neutron diffraction study, *Chem. Mater.* **2002**, *14*, 2063-2070
- (18) Stoeva, Z.; Jäger, B.; Gomez, R.; Messaoudi, S.; Ben Yahia, M.; Rocquefelte, X.; Hix, G.B.; Wolf, W.; Titman, J.J.; Gautier, R.; Herzig, P.; Gregory, D.H. Crystal chemistry and electronic structure of the metallic lithium ion conductor, LiNiN , *J. Am. Chem. Soc.* **2007**, *129*, 1912-1920
- (19) Yamada, A.; Matsumoto, S.; Nakamura, Y. Direct solid-state synthesis and large-capacity anode operation of $\text{Li}_{3-x}\text{Fe}_x\text{N}$, *J. Mat. Chem.* **2011**, *21*, 10021-10025
- (20) Li, G.; Xue, R.; Chen, L. The influence of polytetrafluoroethylene reduction on the capacity loss of the carbon anode for lithium batteries, *Solid State Ionics* **1996**, *90*, 221-225
- (21) Kavan, L. Electrochemical carbon, *Chem. Rev.* **1997**, *97*, 3061-3082
- (22) Klatyk, J.; Höhn, P.; Knip, R. Crystal structure of pentalithium tris[nitridolithiate/niccolate], $\text{Li}_5[(\text{Li}_{1-x}\text{Ni}_x)\text{N}]_3$ ($x=0.77$), *Z. Krist. NCS* **1998**, *213*, 31
- (23) Niewa, R.; Wagner, F. R.; Schnelle, W.; Hochrein, O.; Knip, R. $\text{Li}_{2.4}[\text{MnN}_3]_3\text{N}_2$ and $\text{Li}_5[(\text{Li}_{1-x}\text{Mn}_x)\text{N}]_3$, two intermediates in the decomposition path of $\text{Li}_7[\text{MnN}_4]$ to $\text{Li}_2[(\text{Li}_{1-x}\text{Mn}_x)\text{N}]$: an experimental and theoretical study, *Inorg. Chem.* **2001**, *40*, 5215

For Table of Contents Only.

The layered lithium nitridonickelate $\text{Li}_{2.0}\text{Ni}_{0.67}\text{N}$ exhibits a particularly stable specific capacity of 200 mAh g^{-1} . Its structural response explains the $\text{Li}_{2.0}\text{Ni}_{0.67}\text{N}$ excellent cycling life. A solid-solution type response is evidence from operando XRD with the occurrence of in-plane supercell to accommodate the lithium vacancies created during the oxidation. Such a structural response is perfectly reversible.

